 CMC, vol.32, no.3, pp.159-176, 2012

A Loose Coupling Multiscale Approach for the Detailed Analysis of the Influence of Critical Areas on the Global Behaviour of Composite Structures

D. Chrupalla[1], J. Kreikemeier[1], S. Berg[2], L. Kärger[3], M. Doreille[4] T. Ludwig[4], E. Jansen[2], R. Rolfes[2] and A.Kling[1]

Abstract: In this paper, a loose coupling multiscale modeling technique for the detailed numerical analysis of critical areas in composite structures is presented. It is used to describe the global (macroscopic) behaviour of composite structures taking into account the effects of local phenomena. This is done by indirectly connecting the global and local FE-models. Prescribed displacements are assigned to the local boundaries in the transition from the global to local modeling level. The local-to-global transition is realized by assigning averaged local stresses to the respective global Gauss points and by updating the global tangent stiffness operator. To illustrate the feasibility of the approach and to verify its implementation in the commercial FE code ABAQUS^{TM} by user-defined subroutines and scripts, a test case for a solid-to-solid coupling has been investigated. A comparison of the results of the multiscale approach with numerical reference solutions shows that the implementation works appropriate.

Keywords: Multiscale modeling, RVE, homogenization.

1 Introduction

Composite materials have gained a large influence in the aircraft industry over the last decades due to their high specific stiffness and strength. Still, a lot of challenges have to be met in the design stage. Computationally efficient failure analysis tools have to be developed to achieve an economical and reliable design of composite aircraft structures. By the suitable combination of large scale or macroscopic and

[1] German Aerospace Centre (DLR), Institute of Composite Structures and Adaptive Systems, Germany, david.chrupalla@dlr.de , janko.kreikemeier@dlr.de , a.kling@dlr.de

[2] Leibniz Universität Hannover, Institute of Structural Analysis, Germany, s.berg@isd.uni-hannover.de, e.jansen@isd.uni-hannover.de, r.rolfes@isd.uni-hannover.de

[3] Karlsruhe Institute of Technology, Germany, luise.kaerger@kit.edu

[4] SMR S.A. (SMR), C.P. 4014, CH-2500 Bienne 4, Switzerland, info@smr.ch

small scale or microscopic FE models, multiscale FE analysis satisfies this demand. The idea is to combine the advantages of two or more modeling levels. Sufficiently accurate results are obtained at the global scale at reasonable computational cost without omitting the influence of relevant physical phenomena at the smaller scale. Such phenomena include process-induced defects like porosity, fibre waviness or micro-cracks in the matrix material. In the context of multiscale modeling, the term "loose coupling" refers to the indirect connection of structural FE-models of different fidelity and refinement. The global model and all local submodels are described by different systems of equations, which are solved separately. In a "tight coupling" approach on the other hand, the local submodels are integrated into the global model such that only one system of equations is solved.

Multiscale modeling techniques can be used to describe the macroscopic behaviour of heterogeneous materials like composite materials or materials with defects which are much smaller than the structural dimensions. The most common method for the definition of complex microstructures today is given by the representative volume element (RVE) approach in conjunction with a numerical homogenization scheme, Nemat-Nasser, S. (1999), Lubarda, V. (2002) or Böhlke, T. (2001). When dealing with multiscale modeling strategies, the dimensions on the micro scale must be orders of magnitudes smaller compared to the structural dimensions, i.e., $L_{Micro} \leq L_{Macro}$. Thus, the assumption of scale separation is fulfilled. The scale separation as well as the homogenization scheme are point wise procedures, i.e., the effective material behavior of one macroscopical material point is obtained by means of a RVE of finite size, Kreikemeier, J. (2011).

In general the distinction between uncoupled as well as coupled homogenization schemes can be made. The uncoupled approach is used in case of linear elastic materials and small deformations to obtain the effective response just once, Suquet, P. (1987), whereas the coupled approach should be used in case of finite deformations and inelastic material behavior, e.g., to describe plasticity or damage phenomena, Schröder, J. (1996), Miehe, C.; Schotte, J.; Lambrecht, M. (2002), Kouznetsova, V. (2002) or Gitman, I. (2006). In contrast to the uncoupled homogenization scheme, for the coupled approach at any time both the microscopic as well as the macroscopic boundary value problem must be solved simultaneously, because the effective material response is highly dependent on the actual microscopic behavior. Hence a smart solution strategy should be used to save computational resources.

If the assumption of scale separation does not hold anymore, the scale transition can be defined by using hierarchical multiscale approaches. In interesting macroscopic regions, a fine discretization of the whole underlying microstructure is made, see for example, Fish, J. (1992), Hughes, T.; Feijóo, G.; Mazzei, L.; Quincy, J. (1998), Kadowaki, H.; Liu, W. (2004) or Gitman, I. (2006).

In Feyel, F. (2003) and Feyel, F. (1999), an FE^2 approach is developed and implemented into a general purpose finite element program. They introduce a two scale approach to obtain the effective constitutive response of the macroscopic region. This approach is named FE^2 because a simultaneous finite element computation of the mechanical response at two different length scales is carried out at each macroscopic integration point. The whole approach is handled as a classical internal variable model where the internal variables are taken from the microscopic data which are required by the microscopic RVE calculation.

In Kouznetsova, V. (2002), a multilevel FE method is developed to account for the visco-plastic behavior of an aluminum material with a certain amount of voids. The focus of this work lies on the higher order homogenization scheme by use of gradients of the deformation measures within the constitutive relation.

In Miehe, C.; Schotte, J.; Lambrecht, M. (2002), a continuous as well as a discrete variational formulation for the homogenization of inelastic materials at finite strains are developed by using an energy storage function as well as a dissipation function to account for the effective response of a general standard medium.

In Kim, B.; Lee, H. (2010), a micromechanical elasto-plastic damage model in conjunction with a RVE formulation is presented to get the overall damage behavior of fiber reinforced matrix composites. The approach is based on an exterior point Eshelby tensor for circular inclusion problems, see Li, S.; Sauer, R.; Wang, G. (2005), and the ensemble-averaged effective yield criterion.

As a result, when using multiscale material modeling strategies the computational effort is very large, but by a detailed description of all of the micromechanical features as well as the ongoing improvements of computational power and performance the research within this field is justified.

In this paper, a multiscale modeling technique for an automated iterative loose coupling approach is presented. It is used to describe the macroscopic behaviour of composite structures. The global-to-local transition is realized via prescribed displacements at the microscopic boundary nodes, whereas the local-to-global transition is realized by assigning averaged stresses obtained from the solution of the local boundary value problem to the respective integration points at the global level and updating the global tangent stiffness operator for the global Newton-Raphson scheme. Specific hotspot-criteria are used to decide when and where a local model needs to be generated.

The presented automated iterative multiscale approach is a step beyond state-of-the-art, since at present the developments of loose coupling are still at the beginning and limited to non-automatic and one-step procedures like classical FE substructuring algorithms. Furthermore, this multiscale method, denoted as “Homogenization-

based two-way multiscale approach" (HIMSA), enables local investigation not only of single global material points as usually performed in homogenization procedures, but also of larger critical areas of the global model. The exchange between the models of different scale is performed by a two-way coupling, i.e. from global to local and back to global. Thus, the effects of local phenomena on the global behaviour of a structure are taken into account.

The methodology of the loose coupling approach is presented in Chapter 2. In chapter 3, the feasibility of this approach in the commercial FE code ABAQUS^{TM} is demonstrated with a test case. To check for the correctness of the implementation, the obtained results are compared to the results from a verification calculation. In chapter 4, the main results of the work are summarized and an outlook on the next steps is given.

2 Homogenization-based iterative two-way multiscale approach (HIMSA)

In the homogenization-based iterative two-way multiscale approach (HIMSA), the scales of the local and the global model are different in the sense that the local model is small with respect to the global model. However, in general the dimensions of the local model are not an order of magnitude smaller than the dimensions of the global model, and therefore in the presented approach, a volumewise transfer of information is used between the different levels. This situation is different from the pointwise transfer that is often used for material homogenization, where scales are distinctly separate (see Aboudi, J. (1991) or Böhlke, T. (2001)). The steps for HIMSA can be formulated as follows:

- Definition of the local model (via hotspot criterion/criteria)
- Global-to-local transition: Formulation of boundary conditions for the local model from input variables of the global model (nodal displacements u_M)
- Solution of the local boundary value problem
- Local-to-global transition: Solution of the boundary value problem of the local model and calculation of global output variables (averaged stresses)
- Numerical determination of the global tangent stiffness operator

2.1 Definition of the local model

As a first step the global area has to be chosen, which shall be investigated closely via a local model. This will be done by the use of the failure criterion proposed by Hashin as a hot-spot criterion, Hashin, Z. (1980). By this criterion a distinction

between fibre failure due to tension or compression and matrix failure due to tension or compression is possible:

$$\left(\frac{\sigma_{11}}{R_{||}^{(+)}}\right)^2 + \frac{1}{R_{\perp||}^2}\left(\sigma_{12}^2+\sigma_{13}^2\right) \geq 1 \text{ for } \sigma_{11} > 0 \tag{1}$$

$$\left(\frac{\sigma_{11}}{R_{||}^{(-)}}\right)^2 \geq 1 \text{ for } \sigma_{11} < 0 \tag{2}$$

$$\begin{aligned}&\tfrac{1}{R_{\perp}^{(+)2}}\left(\sigma_{22}+\sigma_{33}\right)^2 + \tfrac{1}{R_{\perp\perp}^2}\left(\sigma_{23}^2-\sigma_{22}\sigma_{33}\right) + \\ &\tfrac{1}{R_{\perp||}^2}\left(\sigma_{12}^2+\sigma_{13}^2\right) \geq 1 \text{ for } \sigma_{22}+\sigma_{33} > 0\end{aligned} \tag{3}$$

$$\begin{aligned}&\tfrac{1}{R_{\perp}^{(-)}}\left[\left(\tfrac{R_{\perp}^{(-)}}{2R_{\perp\perp}}\right)^2 - 1\right]\left(\sigma_{22}+\sigma_{33}\right) + \tfrac{1}{4R_{\perp\perp}^2}\left(\sigma_{22}+\sigma_{33}\right)^2 + \\ &\tfrac{1}{R_{\perp\perp}^2}\left(\sigma_{23}^2-\sigma_{22}\sigma_{33}\right) + \tfrac{1}{R_{\perp||}^2}\left(\sigma_{12}^2+\sigma_{13}^2\right) \geq 1 \\ &\text{for } \sigma_{22}+\sigma_{33} < 0\end{aligned} \tag{4}$$

Here, σ_{ij} denote the components of the Cauchy stress tensor and R are the material strengths for tension (+), compression (-) and shearing.

Adjacent critical global elements are merged to one large local model. This procedure is appropriate if several critical global elements are located in the same global area. Thus, the local model represents not only one global material point but an area of the global model. Nevertheless the local model is much more detailed, e.g. in terms of the material model, and has a finer mesh compared to the global one.

2.2 Global-to-local transition

For the transition from global to local level, the displacements of the global nodes at the boundary of the local model are used as boundary conditions for the local model. The inner local nodes remain unrestrained. Local boundary nodes that coincide with a global node get the exact value of the global nodal displacement. The nodal displacements at the other local boundary nodes which lie in between the global nodes are interpolated via the global shape functions N of the global finite element type used. In ABAQUS^{TM} , no information about the current displacement field can be obtained directly. Thus, the displacements at the global nodes have to be calculated from the strain field at the global Gauss points. In the studies in this paper, small deformations are assumed. As a consequence, higher order terms in

the strain tensor are neglected and the strain tensor equals the symmetric part of the displacement gradient:

$$\mathbf{E}_{\mathrm{M}}^{\mathrm{L}} = \frac{1}{2}\left(\mathbf{H}_{\mathrm{M}} + \mathbf{H}_{\mathrm{M}}^{\mathrm{T}}\right) \tag{5}$$

$\mathbf{E}^{L}{}_{M}$ – Linearized Green-Lagrange strain tensor at the global level

$\mathbf{H}_{M}$ – Displacement gradient at the global level

The displacement field at the global Gauss-Points is calculated via:

$$\mathbf{u}_{\mathrm{Gauss}} = \mathbf{E}_{\mathrm{M}}^{\mathrm{L}} \cdot \mathbf{x_0} \tag{6}$$

$\mathbf{u}_{Gauss}$ – Displacement at one global Gauss point

$\mathbf{x}_0$ – Coordinates of the global Gauss point

After the inversion of the global element shape functions, the displacement field at the global nodes is calculated as:

$$\mathbf{u}_{\mathrm{node}} = \mathbf{N}^{-1} \cdot \mathbf{u}_{\mathrm{Gauss}} \tag{7}$$

$\mathbf{u}_{node}$ – Vector of displacements at the global nodes

$\mathbf{N}$ – Matrix of global element shape functions

The interpolation of displacements at the local edge nodes in between global nodes is calculated as:

$$\mathbf{u}_{\mathrm{localnode}} = \mathbf{N}_{\mathrm{localnode}} \cdot \mathbf{u}_{\mathrm{node}} \tag{8}$$

$\mathbf{u}_{localnode}$ – Vector of displacements at the local boundary nodes

$\mathbf{N}_{localnode}$ – Matrix of global element shape functions values at locations of local nodes

2.3 Solution of the local boundary value problem

For the critical area at the local level, the material behaviour is defined to be non-linear. A material model developed in Hartung, D. (2009) based on the model developed by Ladevèze, P.; Le Dantec, E. (1992) has been developed further and implemented into a Fortran coded subroutine in ABAQUS^{TM} (UMAT). With this approach, the intralaminar and interlaminar behaviour of the laminate can be modeled without discretization of the interfaces between the plies. This leads to a reduction of the numerical effort. The model by Hartung, D. (2009) has been developed and validated for a non crimp fabric (NCF) material with a [0/90] layup. In that

model, the assumption holds that interlaminar shear loads cause shear damage in fibre direction and lateral to the fibres. This is why only one interlaminar shear damage variable d_{23} is used in the model. In case of a laminate with an arbitrary layup, this assumption holds no longer and the interlaminar shear damage in fibre direction and lateral to the fibres have to be treated separately.

2.3.1 Internal energy of the damaged material

The model bases on the energy definition of the damaged material. The strain energy E_D is defined as:

$$E_D = \frac{1}{2}\left[\begin{array}{l} \frac{\sigma_{11}^2}{E_{11}(1-d_{11})} + \frac{\langle\sigma_{22}\rangle^2}{E_{22}(1-d_{22})} - \frac{\langle-\sigma_{22}\rangle^2}{E_{22}} + \frac{\langle\sigma_{33}\rangle^2}{E_{33}(1-d_{33})} \\ + \frac{\langle-\sigma_{33}\rangle^2}{E_{33}} - \left(\frac{\nu_{12}}{E_{11}} + \frac{\nu_{21}}{E_{22}}\right)\sigma_{11}\sigma_{22} - \left(\frac{\nu_{13}}{E_{11}} + \frac{\nu_{31}}{E_{33}}\right)\sigma_{11}\sigma_{33} \\ - \left(\frac{\nu_{23}}{E_{22}} + \frac{\nu_{32}}{E_{33}}\right)\sigma_{22}\sigma_{33} + \frac{\tau_{12}^2}{G_{12}(1-d_{12})} + \frac{\tau_{13}^2}{2G_{13}(1-d_{13})} + \frac{\tau_{23}^2}{2G_{23}(1-d_{23})} \end{array}\right] \tag{9}$$

The material exhibits orthotropy. Material damage is described via damage variables d_{ij}, that degrade the material stiffnesses with increasing load. The material behaviour lateral to the fibre direction is modeled separately for the cases of tension and compression. Compression loads do not cause material damage directly.

2.3.2 Energy release rates

Damage evolution is characterized by the energy that is necessary for a progression of the damage. These state variables Y_{ij} associated with the damage variables are calculated from the energy E_D. For damage caused by normal loads, the energy release rates are calculated as:

$$Y_{11} = \left.\frac{\partial E_D}{\partial d_{11}}\right|_{\sigma} = \frac{1}{2}\frac{\sigma_{11}^2}{E_{11}\left(1-d_{11}\right)^2} \tag{10}$$

$$Y_{22} = \left.\frac{\partial E_D}{\partial d_{22}}\right|_{\sigma} = \frac{1}{2}\frac{\langle\sigma_{22}\rangle^2}{E_{22}\left(1-d_{22}\right)^2} \tag{11}$$

$$Y_{33} = \left.\frac{\partial E_D}{\partial d_{33}}\right|_{\sigma} = \frac{1}{2}\frac{\langle\sigma_{33}\rangle^2}{E_{33}\left(1-d_{33}\right)^2} \tag{12}$$

For shear damage, the energy release rates are calculated as:

$$Y_{12} = \left.\frac{\partial E_D}{\partial d_{12}}\right|_{\sigma} = \frac{\tau_{12}^2}{2G_{12}\left(1-d_{12}\right)^2} \tag{13}$$

$$Y_{13} = \left.\frac{\partial E_D}{\partial d_{13}}\right|_{\sigma} = \frac{\tau_{13}^2}{2G_{13}\left(1-d_{13}\right)^2} \tag{14}$$

$$Y_{23} = \left.\frac{\partial E_D}{\partial d_{23}}\right|_{\sigma} = \frac{\tau_{23}^2}{2G_{23}\left(1-d_{23}\right)^2} \tag{15}$$

According to Phillips, E.A.; Herakovich, C.T.; Graham, L.L. (2001), it is reasonable to couple the intralaminar damage lateral to the fibre direction with the intralaminar shear damage. The intralaminar matrix damage is calculated by a combined function:

$$Y_{22}^h(t) = \sup_{\tau \le t}\left(Y_{12}(\tau) + bY_{22}(\tau)\right) \text{ with } b = \frac{E_{22}}{G_{22}} \tag{16}$$

The supremum function prevents the damaged material from healing. Analogously, for the remaining energy release rates the maximum values in the load history are taken into account:

$$Y_{11}(t) = \sup_{\tau \le t}\left(Y_{11}(\tau)\right) \tag{17}$$

$$Y_{33}(t) = \sup_{\tau \le t}\left(Y_{33}(\tau)\right) \tag{18}$$

$$Y_{13}(t) = \sup_{\tau \le t}\left(Y_{13}(\tau)\right) \tag{19}$$

$$Y_{23}(t) = \sup_{\tau \le t}\left(Y_{23}(\tau)\right) \tag{20}$$

Figure 1 shows the scheme of the model. Intralaminar and interlaminar damage are uncoupled. Fibre failure is treated separately while intralaminar damage lateral to the fibre direction is calculated from a combined inner thermodynamical force.

2.3.3 Damage evolution

Material damage does not occur until a certain threshold value is reached. The state ${Y^0}_{ij}$ is the limit between a completely undamaged and damaged material and is taken into account in the damage evolution functions. Once this threshold value is reached, the material stiffness is degraded. The stiffness degradation continues with increasing load until the maximum energy release rate ${Y^r}_{ij}$ is reached. This material parameter characterizes the state, when the maximum damage in the material is reached, which leads to complete failure. The material stiffness is then degraded almost completely.

In case of loading in fibre direction, the maximum energy release rates are defined by means of the tensile and compressive strength ${R^{(+)}}_{11}$ and ${R^{(-)}}_{11}$:

$$Y_{11}^{rt} = \frac{1}{2}\frac{R_{11}^{(+)2}}{E_{11}}, \quad Y_{11}^{rc} = \frac{1}{2}\frac{R_{11}^{(-)2}}{E_{11}} \tag{21}$$

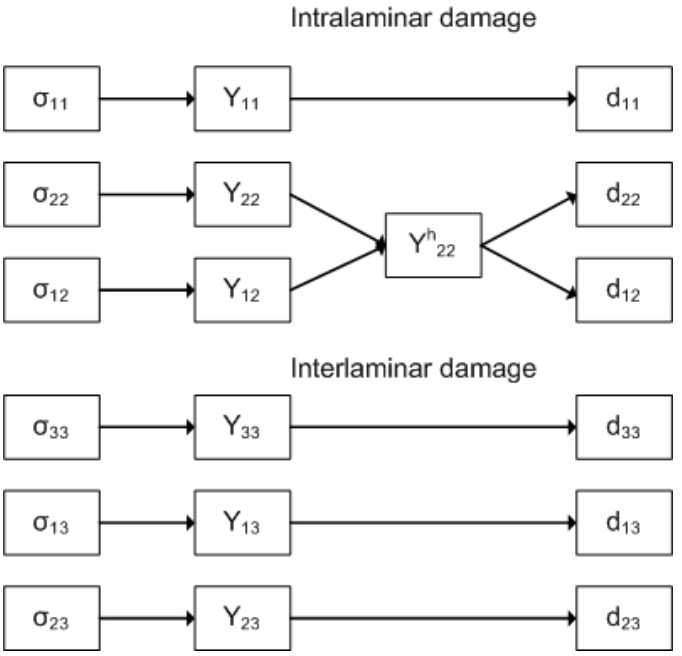

Figure 1: Scheme of the damage model

No damage evolution is considered in this case, i.e. the material behaviour is assumed to be purely linear elastic before failure.

The maximum energy release rates for intralaminar matrix failure and interlaminar failure under normal and shear load are calculated from experimentally determined material strength values ${R^F}_{ij}$ and damage ${d^F}_{ij}$. This is done by means of static, multi-level, cyclic load tests as described in Ladevèze, P.; Le Dantec, E. (1992):

$$Y_{22}^r = \frac{1}{2}\frac{R_{22}^{(+)2}}{E_{22}\left(1-d_{22}^F\right)^2}, Y_{12}^r = \frac{1}{2}\frac{{R_{12}^F}^2}{G_{12}\left(1-d_{12}^F\right)^2}, \tag{22}$$

$$Y_{33}^r = \frac{1}{2}\frac{R_{33}^{(+)2}}{E_{33}\left(1-d_{33}^F\right)^2}, \quad Y_{13}^r = \frac{1}{2}\frac{{R_{13}}^2}{G_{13}\left(1-d_{13}^F\right)^2}, \quad Y_{23}^r = \frac{1}{2}\frac{{R_{23}}^2}{G_{23}\left(1-d_{23}^F\right)^2}$$

Generally, the damage of the material progresses when the load is increased. Due to the brittle behaviour in fibre direction, only the undamaged or the fully damaged state are distinguished. It is checked if the maximum energy release rate for tensile

or compression load is exceeded. Between these two states, the material is undamaged. This leads to the formulation for the damage evolution in fibre direction:

$$\omega_{11} = d_{11} = \begin{cases} 0 & \text{if } -Y_{11}^{rc} < Y_{11} < Y_{11}^{rt} \\ 1 & \text{else} \end{cases} \tag{23}$$

The intralaminar damage evolution function is of hyperbolic character:

$$\omega_{22} = \begin{cases} \frac{\left\langle \sqrt{Y_{22}^h} - \sqrt{Y_{22}^0} \right\rangle}{\sqrt{Y_{22}^c}} & \text{if } Y_{22} \leq Y_{22}^r, \\ 1 & \text{else} \end{cases} \tag{24}$$

$$\omega_{12} = \begin{cases} \frac{\left\langle \sqrt{Y_{22}^h} - \sqrt{Y_{12}^0} \right\rangle}{\sqrt{Y_{12}^c}} & \text{if } Y_{12} \leq Y_{12}^r, \\ 1 & \text{else} \end{cases} \tag{25}$$

The interlaminar damage evolution is defined as:

$$\omega_{33} = \begin{cases} \left[\frac{n}{n+1} \frac{\left\langle Y_{33} - Y_{33}^0 \right\rangle}{Y_{33}^c - Y_{33}^0} \right]^n & \text{if } Y_{33} \leq Y_{33}^r, \\ 1 & \text{else} \end{cases} \tag{26}$$

$$\omega_{13} = \begin{cases} \left[\frac{n}{n+1} \frac{\left\langle Y_{13} - Y_{13}^0 \right\rangle}{Y_{13}^c - Y_{13}^0} \right]^n & \text{if } Y_{13} \leq Y_{13}^r, \\ 1 & \text{else} \end{cases} \tag{27}$$

$$\omega_{23} = \begin{cases} \left[\frac{n}{n+1} \frac{\left\langle Y_{23} - Y_{23}^0 \right\rangle}{Y_{23}^c - Y_{23}^0} \right]^n & \text{if } Y_{23} \leq Y_{23}^r, \\ 1 & \text{else} \end{cases} \tag{28}$$

2.3.4 Regularisation

To avoid localisation phenomena and mesh dependencies due to the material nonlinearities, a regularisation scheme has been proposed by Allix, O.; Feissel, P.; Thévenet, P. (2003) to ensure the stability of the model. By introducing an internal length scale a and a critical time t_c, an artificial viscosity is added to the damage evolution law. The additional equation has the form

$$\overset{\bullet}{d}_{ij} = \frac{1}{t_c} \left[1 - \exp\left(-a \left(\omega_{ij} - d_{ij} \right) \right) \right] \tag{29}$$

This partial differential equation is solved numerically in each iteration of the Newton-Raphson scheme. The internal length scale a is the characteristic element length given by the FE-solver, the critical time t_c is the time step width of the current increment.

2.4 Local-to-global transition

The transition from local to global level is realized by averaging the local stresses over the respective volume of the sub-domain. Each Gauss point of one global element is assigned one local sub-domain. Thus, for each global Gauss point a separate averaged stress tensor is calculated. In case of small deformations, the following simplifying assumption is justified:

$$\mathbf{T}_{\mathrm{m}} \approx \mathbf{P_m} \approx \mathbf{S_m} \tag{30}$$

$\mathbf{T}_m$ – Cauchy stress tensor at the local level

$\mathbf{P}_m$ – First Piola-Kirchhoff stress tensor at the local level

$\mathbf{S}_m$ – Second Piola-Kirchhoff stress tensor at the local

Based on equation (30), the second Piola-Kirchhoff stress tensor at the global level is calculated by averaging the stresses at the local level:

$$\mathbf{S}_{\mathrm{M}} = \frac{1}{\mathrm{V}_{\mathrm{Sub}}} \int_{\mathrm{V}_{\mathrm{Sub}}} \mathbf{S}_{\mathrm{m}} \mathrm{dV}_{\mathrm{Sub}} \tag{31}$$

$$\mathbf{S}_{\mathrm{M}} = \frac{1}{\mathrm{V}_{\mathrm{Sub}}} \sum_{\mathrm{i}=1}^{\mathrm{Np}} (\mathbf{S}_{\mathrm{mi}} \mathrm{V}_{\mathrm{mi}}) \tag{32}$$

$\mathbf{S}_M$ – Second Piola-Kirchhoff stress tensor of one global Gauss point

$\mathbf{S}_{mi}$ – Second Piola-Kirchhoff stress tensor of the local Gauss points i

V_{sub} – Reference volume of the local sub-domain

V_{mi} – Volume associated with local integration point i

$\mathbf{N}_p$ – Number of Gauss points of the local sub-domain.

Analogously, the global Cauchy or first Piola-Kirchhoff stress tensor can be calculated.

2.5 Calculation of the global tangent stiffness

The global analysis exhibits material nonlinearity due to material damage and degradation at the local scale. Thus, a numerically determined tangent stiffness operator for the global Newton-Raphson scheme has to be calculated in each increment. In case of small deformations, the assumption according to the following equation is justified:

$${}^4\mathbf{C}_{\mathrm{M}}^{\mathrm{S}} = \frac{\mathrm{d}\mathbf{S}_{\mathrm{M}}}{\mathrm{d}\mathbf{E}_{\mathrm{M}}} \approx {}^4\mathbf{C}_{\mathrm{M}}^{\mathrm{P}} = \frac{\mathrm{d}\mathbf{P}_{\mathrm{M}}}{\mathrm{d}\mathbf{F}_{\mathrm{M}}} \approx {}^4\mathbf{C}_{\mathrm{M}}^{\mathrm{T}} = \frac{\mathrm{d}\mathbf{T}_{\mathrm{M}}}{\mathrm{d}\mathbf{e}_{\mathrm{M}}} \tag{33}$$

$\mathbf{T}_M$ – Cauchy stress tensor at the global level

$\mathbf{P}_M$ – First Piola-Kirchhoff stress tensor at the global level

$\mathbf{S}_M$ – Second Piola-Kirchhoff stress tensor at the global level

$\mathbf{F}_M$ – Deformation gradient at the global level

$\mathbf{e}_M$ – Euler-Almansi strain tensor at the global level

${}^4\mathbf{C}_M$– Global tangent stiffness operator

$()^S$, $()^P$, $()^T$ refer to $\mathbf{S}_M$, $\mathbf{P}_M$, $\mathbf{T}_M$

For the numerical calculation, the differential quotient of equation (33) has to be formed. Six additional local boundary value problems are solved, in which a small strain perturbation $\delta \mathrm{E}_j$ is added to the j-th component of the global strain tensor successively for j=1...6. Thus, the local boundary value problem must be solved additional six times within each global iteration. In matrix notation, the coordinates of the global tangent stiffness operator with respect to an orthonormal basis system become:

$$C^S_{\mathrm{M},ij} = \frac{S_{\delta E\,j,i} - S_{\mathrm{homogenized},i}}{\delta E_j}, \quad i = 1...6, j = 1...6 \tag{34}$$

$\mathrm{C}_M{}^S{}_{ij}$– Components of the global tangent stiffness operator

$\mathrm{S}_{homogenized,i}$– i-th component of second Piola-Kirchhoff stress tensor at one local integration point, obtained from averaging the local stress tensor

$\delta \mathrm{E}_j$– Small perturbation to the j-th component of the global Green-Lagrange strain tensor

$\mathrm{S}_{\delta E\,j,i}$ – i-th component of the perturbed stress tensor

3 Solid-to-solid coupling: a numerical example

In this chapter, a test case for solid-to-solid coupling is investigated. The test case consists of a bar which is subjected to a tension load in its axial direction. Three calculations are carried out: two reference calculations, one with a coarse and one with a fine mesh (both without the coupling of different model levels) and one calculation with the homogenization-based two-way multiscale approach. The goal is to show the feasibility of the approach in the commercial FE code ABAQUS$^{\mathrm{TM}}$ via manual implementation of subroutines and scripts and to verify the implemented homogenization-based two-way multiscale approach.

3.1 Reference calculations

The first reference model with the coarse mesh consists of five linear solid elements with cubical shape and an edge length of 2 mm. The bar is clamped on one side

and a displacement of 0.07 mm in axial direction is applied on the other side. The analysis is geometrically linear. The material properties are orthotropic, see also Table 1. Material nonlinearity is introduced by using the damage model presented in chapter 2.3 in the center element, which is assumed to be the critical area. The axial direction of the bar complies with the 2-direction of the material.

Table 1: Initial material properties [8]

E_{11}	136.000 MPa	G_{12}	4.538 MPa	ν_{12}	0.24
E_{22}	8.574 MPa	G_{13}	4.538 MPa	ν_{13}	0.24
E_{33}	11.195 MPa	G_{23}	4.226 MPa	ν_{23}	0.038

The second reference model has a finer mesh compared to the first one. The elements are of cubical shape with an edge length of 0.5 mm. The remaining model properties are the same as in the reference model with the coarse mesh. The critical area has the same geometry. Figure 2 shows the two FE-models.

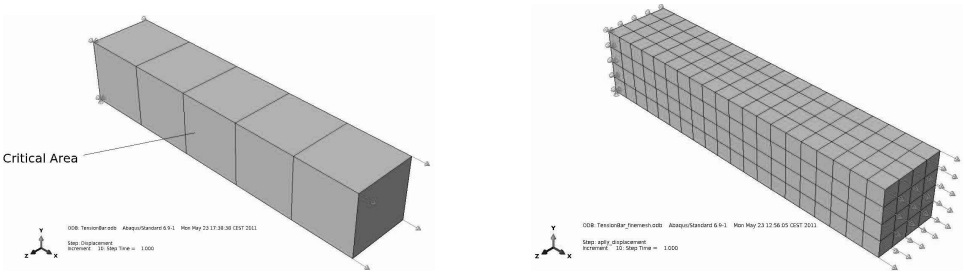

Figure 2: Reference models: Coarse and fine mesh

3.2 Calculation with HIMSA

The global model for the calculation with the homogenization-based two-way multiscale approach has the same geometry, initial material properties and boundary conditions as the reference model with the coarse mesh. The analysis is geometrically linear due to small deformations. The material nonlinearity of the critical area of the bar is modelled by the global-local coupling procedure described in chapter 2. The local model has the geometry of the critical global element in the centre of the bar. The mesh density is the same as for the reference model with the fine mesh. The material nonlinearity at the local level is modelled with the same material model as in the reference calculation. Figure 3 shows an overlay plot of the global and the local model.

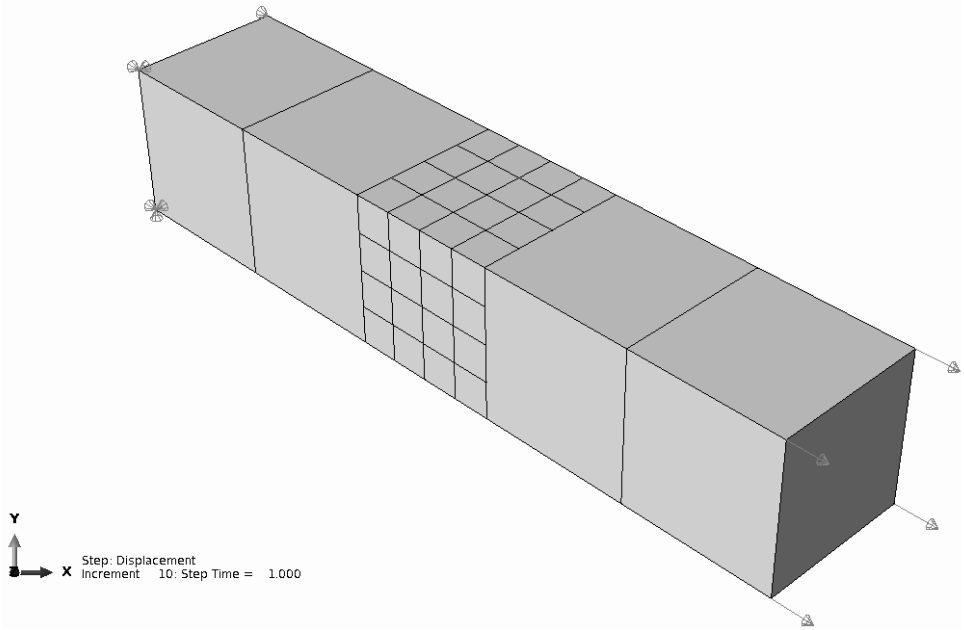

Figure 3: Overlay plot of the global and local model

The global-to-local coupling procedure is carried out if the failure criterion at the global level is fulfilled or has been fulfilled in a previous load increment. The algorithm has the following form:

1. Initialize the global model
2. Begin next global increment
   - Perform prediction for next load increment
   - Compute initial residuum
3. Begin next global iteration
   - Compute initial tangent stiffness
   - Perform correction: Compute displacement field from strains at global Gauss points
4. Calculate stresses from initial material stiffness and strains and check, if global failure criterion is fulfilled or was fulfilled before.
   - If yes: GO TO 5.

- If not: GO TO 2.

5. Create local boundary value problem
6. Solve local boundary value problem
7. Homogenize stresses and assign them to respective global Gauss Points
8. Calculate the global tangent stiffness operator numerically by solving six local boundary value problems with a small perturbation applied successively to the six coordinates of the global strain tensor.
9. Compute updated global residuum.
   - If residuum > eps: GO TO 3b.
   - If residuum < eps: GO TO 2.
   - If residuum < eps and final global increment is reached: Analysis complete.

Twenty load increments were applied in all three calculations to obtain the solution. The load-displacement curves of the three models are depicted in Figure 4. The load increases linearly until abrupt failure. The results obtained from the calculations of the reference models are in good agreement with the results obtained from the calculation with HIMSA. This verifies the implementation of the presented approach in the commercial FE-software ABAQUS^{TM} . Deviations are less than 1% and can be ascribed to numerical inaccuracies resulting from small rounding errors during the calculations.

4 Conclusions

A new automated, iterative multiscale approach has been developed and implemented into the commercial FE software ABAQUS^{TM} . Critical areas identified by a hot spot criterion are investigated in detail by local models. These models are loosely coupled to the global model. By exchanging field quantities between the global and local models in an iterative two-way coupling, the effects of local phenomena on the global behaviour are taken into account. Three calculations of a bar consisting of five linear solid elements subjected to a tension load were carried out: two reference calculations with a coarse and a fine mesh for verification purposes and one calculation with the presented multiscale method. A comparison of the load-displacement curves of the reference calculations and the multiscale approach shows that the implementation works appropriate. Small differences in the predicted failure load were noticed due to numerical inaccuracies.

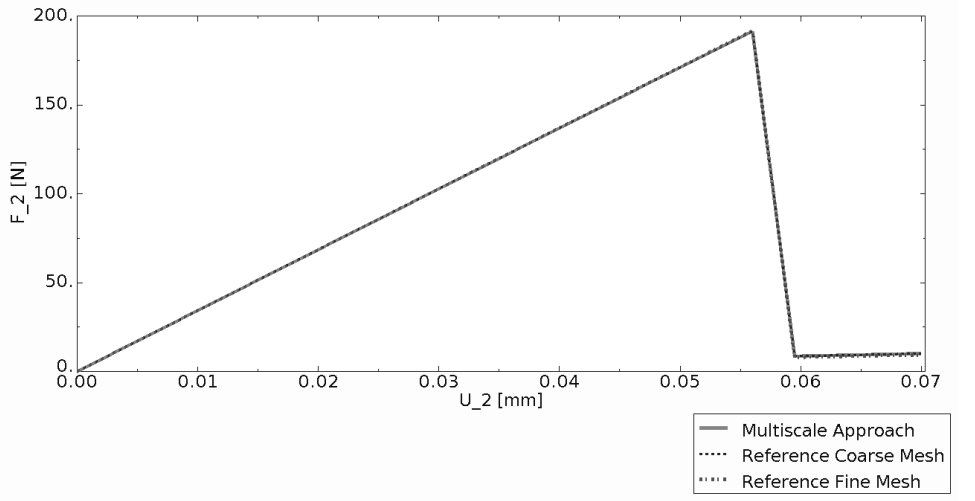

Figure 4: Overlay plot of the global and local model

For the future, the implementation of the approach will be enhanced and applied to geometrically nonlinear problems as well. Moreover two-dimensional shell models shall be coupled to three-dimensional solid models to compute large structures like panels or barrels with this approach.

Acknowledgement: Part of the research leading to these results has received funding from the European Community's Seventh Framework Programme (FP7/2007-2013) under grant agreement n°234147.

5 References

ABAQUSTM (2008) ABAQUSTM Version 6.8 Documentation, ABAQUS 6.8.1.

Aboudi, J. (1991): *Mechanics of composite materials – a unified micromechanical approach.* Elsevier, ISBN 0-4448-8452-1.

Allix, O.; Feissel, P.; Thévenet, P. (2003): A delay damage mesomodel of laminates under dynamic loading: basic aspects and identification issues, *Computers and Structures,* 81, pp. 1177-1191

Böhlke, T. (2001): *Crystallographic Texture Evolution and Elastic Anisotropy – Simulation, Modeling and Application.* Shaker-Verlag, ISBN 3-8265-8758-8.

Chrupalla, D.; Berg, S.; Kärger, L.; Doreille, M.; Ludwig, T.; Jansen, E.; Rolfes, R.; Kling, A. (2011): A homogenization-based Two-way Multiscale Ap-

proach for Composite Materials. Rolfes, R. and Jansen, E. L. (Eds.): *Proceedings of the 3rd ECCOMAS Thematic Conference on the Mechanical Response of Composite Materials*, Institute of Structural Analysis, Leibniz University of Hannover, 2011.

Feyel, F. (2003): A multilevel finite element method (FE^2) to describe the response of highly non-linear structures using generalized continua. *Comp. Meth. Appl. Mech. Engng.*, 192, pp. 3233-3244.

Feyel, F. (1999): Multiscale FE^2 elastoviscoplastic analysis of composite structures. *Comput. Mat. Sci.*, 16, pp. 344-354.

Fish, J. (1992): The s-version of the finite element method, *Computers & Structures*, 43, pp. 539-547.

Garnich, M.R., Karami, G. (2004): Finite Element Micromechanics for Stiffness and Strength of Wavy Fiber Composites. *Journal of Composite Materials*, 38(4), pp. 273-292.

Gitman, I. (2006): *Representative Volumes and Multi-Scale Modelling of Quasi-Brittle Materials.* Technische Universität Delft, 2006.

Hartung, D. (2009): *Materialverhalten von Faserverbundwerkstoffen unter dreidimensionalen Belastungen.* Forschungsbericht DLR 2009-12.

Hashin, Z. (1980): Failure criteria for unidirectional fiber composites, *J. Appl. Mech.*, (47), pp. 329-334

Hsiao, H.M.; Daniel, I.M. (1996): Effect of Fiber Waviness on Stiffness and Strength Reduction of Unidirectional Composites under Compressive Loading. *Composites Science and Technology*, 56(5), pp. 581-593.

Huang, H.; Talreja, R. (2005): Effects of void geometry on elastic properties of unidirectional fiber reinforced composites. *Composites Science and Technology,* 65(13), pp. 1964-1981.

Hughes, T.; Feijóo, G.; Mazzei, L.; Quincy, J. (1998): The variational multiscale method – a paradigm for computational mechanics. *Comp. Meth. Appl. Mech. Engng.*, 166, pp. 3-24.

Jeong, H. (1997): Effects of Voids on the Mechanical Strength and Ultrasonic Attenuation of Laminated Composites. *Journal of Composite Materials*, 31(3), pp. 276-292.

Kadowaki, H.; Liu, W. (2004): Bridging multiscale method for localization problems. *Comp. Meth. Appl. Mech. Engng.,* 193, pp. 3267-3302.

Kim, B.; Lee, H. (2010): Elastoplastic modelling of circular fiber-reinforced ductile matrix composites considering a finite rve. *Int. J. Sol. Struc.,* 47, pp. 827-836.

Kouznetsova, V. (2002): *Computational homogenization for the multi-scale analysis of multiphase materials.* Technische Universität Eindhoven, 2002.

Kreikemeier, J. (2011): *A Two Scale Finite Element Approach to Analyse the Damage State of Composite Structures.* Forschungsbericht DLR 2011-05.

Ladevèze, P.; Allix, O.; Deü, J.F.; Lévêque, D. (2000): A Mesomodel for Localisation and Damage Computation in Laminates. *Comp. Meth. Appl. Mech. Engng.,* 183(1-2), pp. 105-122.

Ladevèze, P.; Le Dantec, E. (1992): Damage modelling of the elementary ply for laminated composites, *Composites Science and Technology,* 43, pp.257-267

Li, S.; Sauer, R.; Wang, G. (2005): A circular inclusion in a finite domain I. The Dirichlet-Eshelby problem. *Acta Mechanica*, 179, pp. 67-90.

Lubarda, V. (2002): *Elastoplasticity Theory.* CRC Press, ISBN 978-0-8493-1138-3.

Miehe, C.; Schotte, J.; Lambrecht, M. (2002): Homogenization of inelastic solid materials at finite strains based in incremental minimization principles. *J. Mech. Phys. Solids,* 50, pp. 2123-2167.

Nemat-Nasser, S. (1999): *Averaging theorems in finite deformation plasticity*, Mech. Mat., 31, pp. 493-523.

Phillips, E.A.; Herakovich, C.T.; Graham, L.L. (2001): Damage development in composites with large stress gradients, *Composites Science and Technology,* 61, pp. 2169-2182

Potter, K.; Khan, B.; Wisnom, M.; Bell, T.; Stevens, J. (2008): Variability, Fibre Waviness and Misalignment in the Determination of the Properties of Composite Materials and Structures. *Composites: Part A,* 39(9), pp. 1343-1354.

Schröder, J. (1996): *Theoretische und algorithmische Konzepte zur phänomenologischen Beschreibung anisotropen Materialverhaltens.* Institut für Mechanik (Bauwesen), Universität Stuttgart, 1996.

Suquet, P. (1987): Elements of homogenization for inelastic solid mechanics. *Homogenization Techniques for Composite Media,* pp. 193-278.